Chemical Physics 62 (1981) 387–405
North-Holland Publishing Company

VIBRATIONAL ENERGY TRANSFER AND RELAXATION PROCESSES IN CH_3Br. A DETAILED KINETIC ANALYSIS OF THE LOWER VIBRATIONAL LEVELS

A.J. OUDERKIRK, V.A. APKARIAN and Eric WEITZ*
Department of Chemistry and Materials Research Center, Northwestern University, Evanston, Illinois 60201, USA

Received 27 May 1981

Energy transfer processes among the lower vibrational levels in CH_3Br have been examined in an attempt to obtain information about the magnitude of the rate constants coupling these levels with one another and coupling ν_3 and ν_6 to the ground state. We conclude that there is a significant direct deactivation of both ν_3 and ν_6 to the ground state for CH_3Br–CH_3Br collisions. The magnitude of V–V rate constants for CH_3Br–CH_3Br and CH_3Br–rare gas interactions are discussed. In the course of these studies, a numerical method has been developed which allows for the determination of kinetic rate constants from measured rates by iterative solution of the coupled set of kinetic equations. Propagation of error from experimental rates to kinetic rate constants has been explicitly considered. The impact of our kinetic analysis and resulting conclusions on previous studies of the methyl halides is also discussed.

1. Introduction

Vibrational energy transfer in polyatomic molecules has been the focus of a large number of experimental and theoretical investigations [1–9]. A primary goal of the experimental studies has been to obtain accurate state-to-state rate constants for vibrational energy transfer and relaxation processes. These rate constants could then be compared to theoretical calculations of rate constants which are normally based on a specific dynamical model. This comparison can be used to formulate theories as well as to test existing theoretical understanding of various energy transfer processes. For a meaningful comparison it is important that theoretically calculated rate constants be compared to rate constants obtained from experimental data rather than to phenomenological rates. An experimental technique that has achieved widespread usage in vibrational energy transfer studies is laser induced fluorescence [5–9]. Using this technique, a molecule may be prepared with excess population in a single vibrational level and the subsequent time evolution of the population of that state monitored. Additionally, the appearance of population in other vibrational states can be monitored. With a sufficient number of independent observations, it is then at least potentially possible to extract kinetic rate constants from these rate measurements. The connection between observed rates and actual rate constants can be made by solving the appropriate kinetic equations. In general, in a multimode system, solution of the complete coupled set of differential rate equations is not tractable. However, by making some well justified approximations, it is often possible to isolate a relatively small number of states from the total vibrational manifold and to treat them as a kinetically independent subsystem. Additionally, it may be kinetically justifiable to collapse a multistate system into a system with significantly fewer states. In either case, the goal is to reduce the system to a small enough number of states such that a solution of the kinetic rate equations becomes manageable. It should be noted that involved in the above procedure is a certain degree of model dependence. The key to a successful kinetic model is

* Alfred P. Sloan Fellow.

0301-0104/81/0000–0000/$02.75

thus to carefully consider the extent to which the approximations made in the model are valid for the system being studied.

Isolation of a subsystem from the total manifold can be done based on a number of criteria. A common case is the exclusion of high lying states whose population is much smaller than the population of the states of interest [6c]. This is equivalent to assuming that equilibration processes among the high lying states present a negligible perturbation on the population of the states of interest.

The collapse of multistate systems into kinetically equivalent systems with fewer states is also possible if significantly different timescales for equilibration exist within a given system. This, in fact, is the assumption that normally makes it possible to treat the multirotational states of a given vibrational level as an equilibrated single state on the vibrational equilibration timescale. Similarly, by this approximation, it is often possible to treat complete manifolds as equilibrated systems with a single deactivation process on a vibration–translation/rotation (V–T/R) timescale [9].

Clearly, detailed solutions of relatively simple systems can be very useful in the interpretation of the behavior of seemingly complex systems. However, care must be taken in modelling systems so that the determined rate constants are representative of the real system.

In this paper we will treat in detail the vibrational energy transfer processes that are operative among the lowest five excited states of CH_3Br. Though CH_3Br has been previously studied [7, 8], we will show that improvements in experimental equipment and kinetic analysis allow for the extraction of a great deal of previously unobtainable information and in particular allow us to determine kinetic rate constants for a number of vibrational energy transfer processes including the V→T/R deactivation processes in the system. The kinetic rate constants for V→T/R deactivation of CH_3Br by CH_3Br and the rare gases ^3He, ^4He, Ne, Ar, Kr and Xe will then be discussed in relation to existing theoretical predictions. The likely effects of such a kinetic reanalysis will be discussed with regard to V→T/R rate constants in other CH_3X systems and a discussion of these effects on the assumed mechanism for deactivation of CH_3X systems will then be considered.

2. Experimental

An energy level diagram for CH_3Br is shown in fig. 1. Fluorescence from the ν_3 mode of CH_3Br was monitored via a Cu:Ge detector following excitation of ν_6 of CH_3Br with the R(14) line of the 10.6 μ CO_2 laser band. The laser parameters and the entire experimental apparatus have been discussed in detail elsewhere [9]. Briefly, the laser was operated at 200 Hz with 1.5–2.0 mJ/pulse and a pulse width of 400–600 ns (fwhm). The Cu:Ge detector was used in conjunction with cooled 13.5 μ and 11.25 μ long pass (l.p.) filters which eliminated

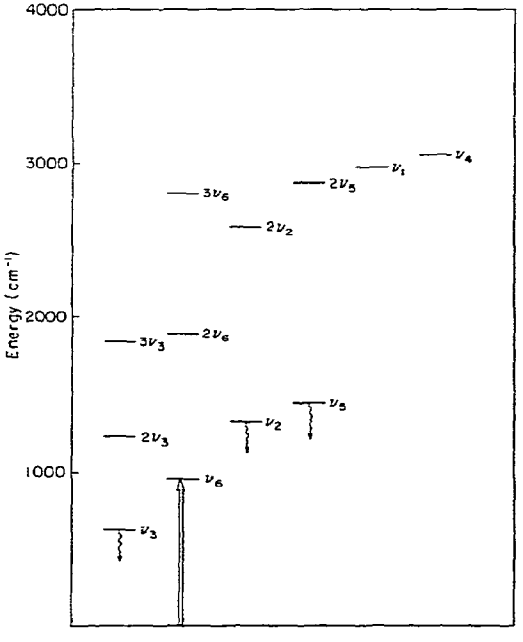

Fig. 1. A partial vibrational energy-level diagram of CH_3Br. The straight arrow indicates the state excited by the CO_2 laser while the curly arrows indicate the states that were monitored in this study.

laser scatter and isolated ν_3 fluorescence emission. Fluorescence was viewed through a KBr window at right angles to the excitation beam. The amplified output of the detector was fed into a Biomation 610B transient digitizer which was interfaced to a hardwired signal averager. The averager was in turn interfaced to either a NOVA 3 or NOVA 4 computer which was linked to a CDC6600 computer.

Fluorescence from the ν_2 and ν_5 modes of CH_3Br was observed with a Au:Ge detector used in conjunction with a 4.8 μ l.p. filter and 7 mm MgF_2 window. This combination provided an optical window of 4.8 to ~8.0 μ. The only CH_3Br modes in this region are ν_2, ν_5, $2\nu_3$ and $2\nu_6$. $2\nu_3$ is very weak in absorption and thus would not be expected to emit significantly. Additionally, any emission would be expected to be attenuated by the long wavelength cut-off of the effective optical window of the detection system. An In:Sb detector was used to verify that there was no significant emission from $2\nu_6$. The In:Sb detector was operated with the same 4.8 μ l.p. filter providing an optical window of 4.8 to ~5.5 μ. Emission from $2\nu_6$ is expected to fall in this region. Within this region, the In:Sb detector used has a higher D^* than the Au:Ge detector and yet no emission could be observed. Therefore, it can be concluded that $2\nu_6$ emission does not make up a perceptible part of the signal observed with the Au:Ge detector within the 4.8 μ to ~8.0 μ optical window. With a 5 kΩ resistive load, the Au:Ge detector and associated electronics had a response time of ≥0.9 μs. When measured signals approached a rate of 500 ms^{-1} a 2 kΩ resistive load was employed with a corresponding increase in response time of the system to ≥0.6 μs [9].

CH_3Br was obtained from Matheson with a specified purity of ≥99.5%. The CH_3Br was further purified by multiple freeze–pump–thaw cycles. All rare gases were used as obtained from the manufacturer. The purity and manufacturers were as follows: ^3He (Mound Labs, ≥99.9%), ^4He (Matheson, ≥99.9999%), Ne (Matheson, ≥99.995%), Ar (Matheson, ≥99.9995%), Kr (Cryogenic Rare Gases, ≥99.995%), and Xe (Cryogenic Rare Gases, ≥99.995%). Rare gas mixtures were prepared in the fluorescence cell and mixing times varied from 5 minutes for He to 20 minutes for Xe. The highest pressure studied for a Xe mixture was 25 Torr. Pressures were measured with a calibrated capacitance manometer on a vacuum line with an outgas/leak rate of 5–10 μ/h.

All experiments were done at 22 ± 1°C. Laser lines were determined by an Optical Engineering CO_2 laser spectrum analyzer.

3. Results

The rise and fall rates of the ν_3 state of CH_3Br were measured for CH_3Br and the rare gases as collision partners. The rise and fall rates of emission from the ν_2 and ν_5 states were also measured. Ronn et al. [8] indicate that in their study the same rates were obtained whether one or both of the ν_2 or ν_5 states were observed. Additionally, these states are expected to be rapidly coupled on the basis of proximity and henceforth will be treated as a single state, ν_2/ν_5.

Typical experimental fluorescence signals from ν_3 and ν_2/ν_5 are presented in figs. 2a and 2b, respectively. The rise and fall rates for both ν_3 and ν_2/ν_5 were analyzed as single exponentials by either a non-linear least-squares routine or an iterative Guggenheim routine. These rates and the pressure ranges of measurement are reported in table 1. Careful attention was paid to the reported error brackets on the measurements which are reported as 95% confidence limits. Our results agree very well with ref. [8] for those states and collision partners that were studied therein. The rates of rise and fall of ν_2/ν_5 and ν_3 are plotted as a function of CH_3Br pressure in figs. 3a and 3b, respectively, for these experiments. A constant pressure of Ar (≈2 Torr) was maintained in the cell in order to increase the overall heat capacity of the system and thus inhibit translational heating. The dependence of the rise and fall rates of ν_3 on Ar pressure is presented in fig. 4. These data are typical of other rare gas measurements. Fig. 5 shows a summary of the experimental rise and

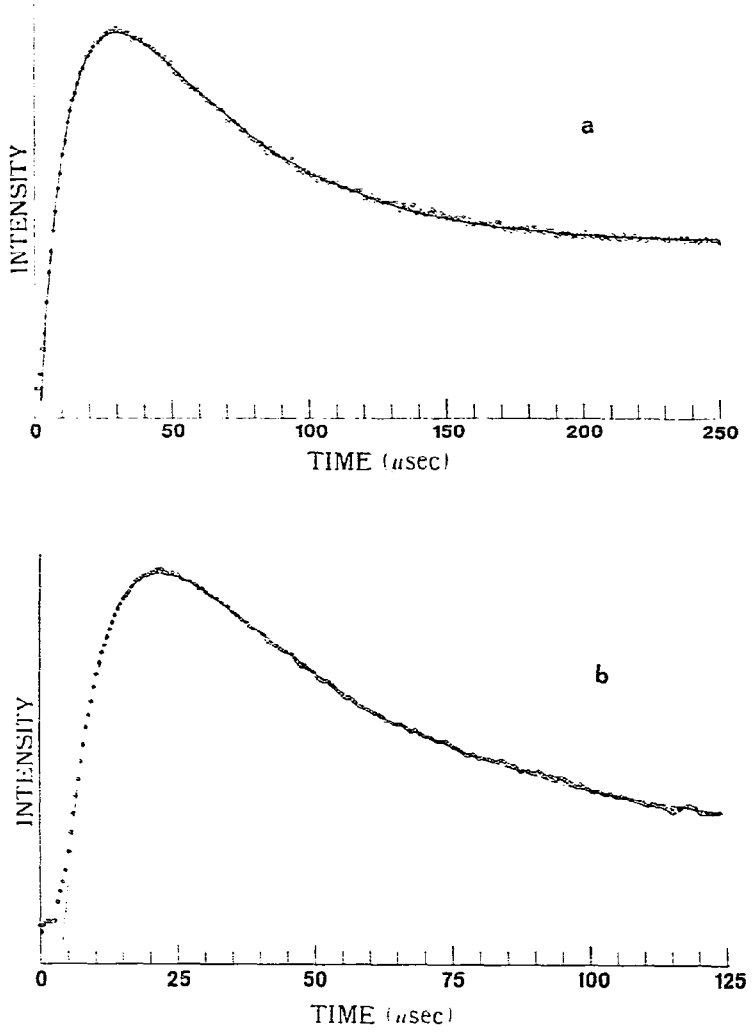

Fig. 2. Typical experimental fluorescence signals from (a) ν_3 and (b) ν_2/ν_5 of CH_3Br. Both signals were obtained from the same gas mixture: 1 Torr of CH_3Br and 2 Torr Ar The continuous line is the double exponential best fit to the signal obtained by a nonlinear least-squares algorithm.

fall rates for ν_3 and ν_2/ν_5 plotted versus $\mu^{1/2}$ of the collision pair.

In a system containing both parent gas, CH_3Br and rare gas the relationship between the rates in the system and the rare gas pressure is not necessarily linear. As discussed in ref. [14], this can occur due to changes in parent–parent versus parent–rare gas V–V and V–T/R rates. Since there was no resolvable deviation from linearity in our rare gas data, a linear least-squares analysis was used to determine rates.

Since, to our knowledge, an iterative Guggenheim procedure has not been previously used

Table 1
Experimental rates of rise and fall of ν_3 and ν_2/ν_5 and pressure ranges for CH_3Br and rare gases as collision partners

Collision partner	State	Pressure range (Torr)	Rate (ms^{-1} $Torr^{-1}$)[a]	
			rise	fall
CH_3Br	ν_3	0.2–1.7	53.3±4.41	19.53±2.72
	ν_2/ν_5	0.3–3	104.5±8.61	22.65±1.95
^3He	ν_3	0–5	34.0±1.81	9.75±0.93
	ν_2/ν_5	0–8	14.6±3.14	9.26±0.63
^4He	ν_3	0–10	18.6±3.15	6.31±1.18
	ν_2/ν_5	0–12.5	12.6±1.47	4.79±0.43
Ne	ν_3	0–30	4.33±0.33	1.63±0.09
	ν_2/ν_5	0–21	6.55±0.80	1.20±0.26
Ar	ν_3	0–30	5.30±0.19	1.85±0.08
	ν_2/ν_5	0–26	7.06±1.66	1.61±0.25
Kr	ν_3	0–25	5.45±0.19	1.60±0.13
	ν_2/ν_5	0–17	8.5 ±1.2	1.67±0.45
Xe	ν_3	0–25	6.06±0.27	1.75±0.16
	ν_2/ν_5	0–17	9.2 ±1.8	2.02±0.40

[a] The reported errors are the 95% confidence limits obtained for the slopes of the rate versus pressure plots.

for data analysis, it was felt that a few comments about this procedure are in order. This analysis extracts the rates and preexponentials from a double exponential curve by performing a single Guggenheim fit [10] for one of the exponentials, subtracting the fitted exponential from the total signal and then performing a Guggenheim fit for the other exponential. The signal is then analyzed a second time where the second exponential is subtracted from the total signal and the first exponential is subjected to a simple Guggenheim analysis. This technique is normally applied iteratively until the results of one iteration do not significantly differ from the results of the previous iteration. The procedure can also be applied to curves containing more than two exponentials. The accuracy of the entire analysis has been confirmed by comparison to an IMSL supplied nonlinear least-squares algorithm (NLSQ). The motivation for using the iterative Guggenheim over the more general NLSQ procedure is that it is significantly faster and therefore more amenable to interactive calculations on a laboratory mini-computer.

4. Discussion

As mentioned previously, some vibrational energy transfer data do exist for the CH_3Br and the CH_3Br–rare gas system. A number of conclusions have been drawn from these previous studies which pertained to the mechanism of vibrational deactivation and in particular seemed to indicate that V→R processes dominated V→T processes in the deactivation mechanism [7]. In addition, a number of theoretical calculations seemed to accurately predict this mechanistic behavior [11, 12]. However, many correlations and comparisons were based on measured experimental rates rather than the actual kinetic rate constants for the vibrational deactivation process. With improved experimental apparatus and more sophisticated kinetic treatments, it seemed appropriate to reinvestigate CH_3Br in an effort to determine the actual kinetic rate constants for vibrational deactivation and to obtain as much additional information as possible about rate constants for V–V processes in the system.

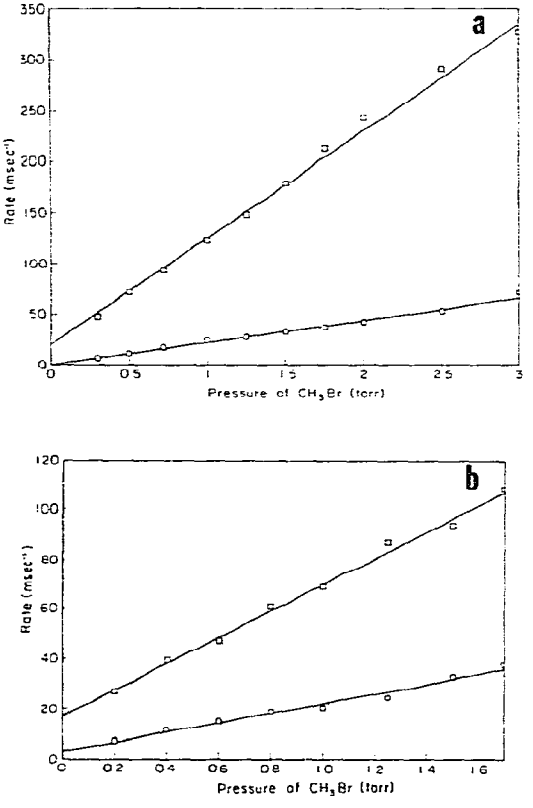

Fig. 3. Observed rate versus pressure plots for (a) ν_2/ν_5 and (b) ν_3. The squares represent rise rates and the circles fall rates. Non-zero intercepts are due to the fact that a constant pressure of Ar (2 Torr) was maintained in the fluorescence cell throughout these experiments in order to inhibit translational heating. The lines are linear least-squares fits to the experimental data.

As previously indicated, when a complete rate matrix for a kinetic system cannot be solved, a simpler kinetic model for the system must be formulated. With a primary interest of this study being the determination of rate constants for deactivation of vibrational degrees of freedom to translational and rotational degrees of freedom, a seemingly plausible first choice for a kinetic model might be a three level system composed of the ground state, ν_3 and the pump state, ν_6.

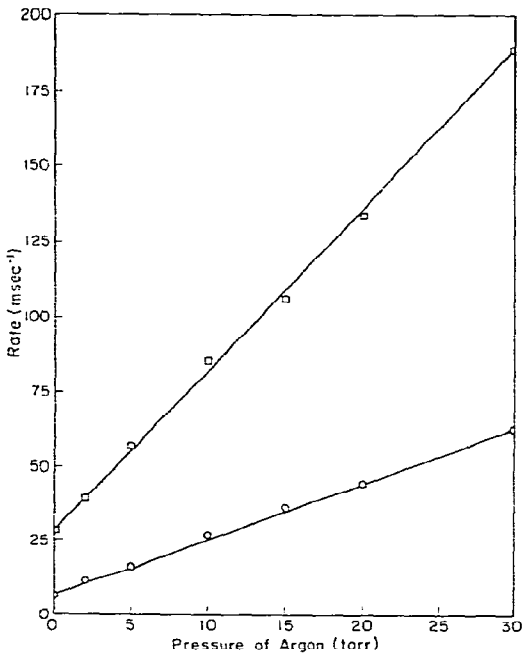

Fig. 4. Rise and fall rates of ν_3 versus pressure of argon. The squares and circles represent the rise and the fall rates, respectively. The pressure of methyl bromide was 0.5 Torr. The solid lines are the result of a linear least-squares fit to the experimental data.

4.1. Three level kinetic model

A simple three level kinetic model involving steps of the type

$$A \underset{k_{-2}}{\overset{k_2}{\rightleftharpoons}} B \underset{k_{-1}}{\overset{k_1}{\rightleftharpoons}} C \qquad (1)$$

has been treated many times since the solutions were first presented by Lowry and John [13]. The solutions for this system and a short discussion will be included here for clarity and convenience.

For CH_3Br the three level system would involve steps of the type

$$CH_3Br(\nu_6) + CH_3Br \underset{k'_{-2}}{\overset{k'_2}{\rightleftharpoons}} CH_3Br(\nu_3) + CH_3Br + \Delta E = 341\ cm^{-1} \qquad (2)$$

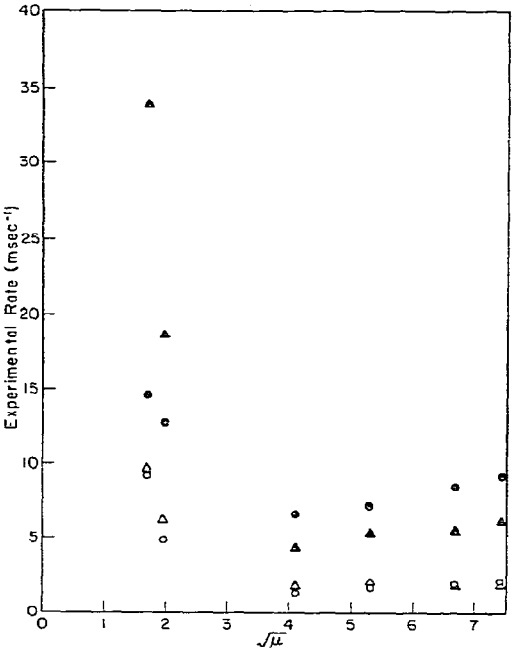

Fig. 5. Summary of the experimental rise and fall rates for ν_3 and ν_2/ν_5 plotted versus $\mu^{1/2}$ of the CH_3Br–rare gas pair: ▲ rise of ν_3, △ fall of ν_3, ● rise of ν_2/ν_5, ○ fall of ν_2/ν_5. The error bars for these measurements are given in table 1.

and

$$CH_3Br(\nu_3)+CH_3Br \underset{k'_{-1}}{\overset{k'_1}{\rightleftharpoons}} CH_3Br(0)+CH_3Br + \Delta E = 611\ \text{cm}^{-1}, \quad (3)$$

for which the rate equations can be written as

$$dN_{\nu_6}/dt = -k'_2 N_{\nu_6} N + k'_{-2} N_{\nu_3} N, \quad (4a)$$

$$dN_{\nu_3}/dt = -k'_1 N_{\nu_3} N + k'_{-1} N_0 N + k'_2 N_{\nu_6} N - k'_{-2} N_{\nu_3} N, \quad (4b)$$

$$dN_0/dt = -k'_{-1} N_0 N + k'_1 N_{\nu_3} N. \quad (4c)$$

additionally, there is the constraint equation

$$N = \sum_{\text{all states}} N_{\nu_i},$$

where N_{ν_i} is the time dependent, pressure weighted population density conveniently normalized such that $N = 1$ at 1 Torr. Using this convention, the bimolecular rate constants, k'_{ν_i}, can be reduced to first order rate constants by making the substitution $k = k'N = k'P$ thus reducing the system to pseudo-first order kinetics where now k_{ν_i} has units of $\text{time}^{-1}\,\text{Torr}^{-1}$.

A rate matrix can be generated for this system and easily solved. The eigenrates of the rate matrix are

$$m_1 = \tfrac{1}{2}[\alpha - (\alpha^2 - 4\beta)^{1/2}], \quad (5a)$$

$$m_2 = \tfrac{1}{2}[\alpha + (\alpha^2 - 4\beta)^{1/2}], \quad (5b)$$

$$m_3 = 0, \quad (5c)$$

where

$$\alpha = k_1 + k_{-1} + k_2 + k_{-2}, \quad (6a)$$

$$\beta = k_1 k_2 + k_2 k_{-1} + k_{-1} k_{-2}. \quad (6b)$$

These eigenrates are independent of the boundary conditions (initial excitation) for the system. In any given experiment, the observed rates are the eigenrates. It can be seen that even for a system as simple as a three level system, the relationship between observed rates and rate constants can be fairly complex. However, once this relationship has been established, experiments can be devised to extract individual rate constants from observed rates.

A complete prediction of the behavior of the different states in the system also requires a knowledge of the eigenvectors, the preexponentials, which depend on boundary conditions. For the case where ν_6 is initially excited the results are

$$\frac{N_{\nu_6}(t)}{N_{\nu_6}(\infty)} = 1 + \frac{k_2(k_{-1}-m_2)m_1}{k_{-1}(k_2-m_2)(m_2-m_1)}\exp(-m_2 t) + \frac{k_2(k_{-1}-m_1)m_2}{k_{-1}(m_1-m_2)(k_2-m_1)}\exp(-m_1 t), \quad (7a)$$

$$\frac{N_{\nu_3}(t)}{N_{\nu_3}(\infty)} = 1 + \frac{(k_{-1}-m_2)m_1}{k_{-1}(m_2-m_1)}\exp(-m_2 t) + \frac{(k_{-1}-m_1)m_2}{k_{-1}(m_1-m_2)}\exp(-m_1 t), \quad (7b)$$

$$\frac{N_{v_3}(t)}{N_{v_3}(\infty)} = 1 + \frac{m_1}{m_2 - m_1}\exp(-m_2 t) + \frac{m_2}{m_1 - m_2}\exp(-m_1 t). \quad (7c)$$

In a determination of rate constants, it is only necessary to measure the pressure dependence of the eigenrates of a state. For the case of ν_6 excitation and observation of ν_3, ν_3 will rise with the faster eigenrate, m_2, and fall with the slower one, m_1. The sum of these eigenrates, $m_1 + m_2$, will yield α and the product, $m_1 m_2$, β. Since k_1 and k_{-1} as well as k_2 and k_{-2} are related by detailed balance and microscopic reversibility, the equations for α and β can be reduced to two unknowns

$$\alpha = (1+\gamma)k_1 + (1+\lambda)k_2, \quad (8a)$$

$$\beta = (1+\lambda\gamma+\gamma)k_1 k_2, \quad (8b)$$

where

$$\lambda = N^0_{\nu_6}/N^0_{\nu_3}, \quad (9a)$$

$$\gamma = N^0_{\nu_3}/N^0_{\nu_0}, \quad (9b)$$

where $N^0_{\nu_i}$ is the ambient Boltzmann population of state i.

The simultaneous solution of these equations results in a quadratic for k_1 which is

$$k_1 = \frac{1}{2}\left\{\frac{\alpha}{1+\lambda} \pm \left[\frac{[\alpha/(1+\lambda)]^2 - 4\beta(1+\gamma)}{(1+\lambda)(1+\lambda\gamma+\alpha)}\right]^{1/2}\right\}. \quad (10)$$

k_2 can then be solved for from either equation (8a) or (8b). For the case where the discriminant of the quadratic is positive, two real sets of rate constants will be obtained. The choice of one set over the other will have to be based on other considerations. The above treatment can be easily extended to the case of the rare gas dependence of the rates of eqs. (2) and (3) and has been treated in a previous publication [14].

Despite the fact that the above treatment is now a standard kinetic procedure, little has been done to relate errors in observed eigenrates to errors in kinetic rate constants. This can be done in a straightforward manner by a study of propagation of errors. This development is presented in appendix A for the three level system.

A point has now been reached where an analysis of the pure CH_3Br and rare gas data for the ν_3 mode of CH_3Br can be attempted based on the simple three level model. Using the data in table 1 and solving for k_1, a disturbing feature is noted. For pure CH_3Br, ^4He, Ne and Ar the discriminant in eq. (10) is negative. In the case of CH_3Br and Ar the discriminant is negative even when the extremes of the error brackets on the rate measurements are considered. This would seem to be a clear indication that a sequential three level mechanism is not an adequate model for the kinetics of this system. Thus, we must consider a model which includes more complex processes as well as more states.

There is theoretical evidence that in the methyl halides there may be some direct deactivation of ν_6 to the ground state in addition to the "normal" V→T/R deactivation process for ν_3 [7, 8, 15]. This is primarily due to the relatively large breathing sphere parameter associated with ν_6 versus ν_3 [7]. In an SSH treatment, this larger breathing sphere parameter can make up, at least in part, for the increased energy gap associated with direct V→T deactivation of ν_6. Thus a natural extension of the previously treated three level system would be to include the process

$$CH_3Br(\nu_6) + CH_3Br \underset{k_{-3}}{\overset{k_3}{\rightleftharpoons}} CH_3Br + CH_3Br(0) + \Delta E = 952\ cm^{-1} \quad (11)$$

in addition to the processes of (2) and (3). The eigenrates for this cyclic system are

$$m_4 = \tfrac{1}{2}[\alpha - (\alpha^2 - 4\beta)^{1/2}], \quad (12a)$$

$$m_5 = \tfrac{1}{2}[\alpha + (\alpha^2 - 4\beta)^{1/2}], \quad (12b)$$

$$m_6 = 0, \quad (12c)$$

where

$$\alpha = k_1 + k_{-1} + k_2 + k_{-2} + k_3 + k_{-3}, \quad (13a)$$

$$\beta = k_{-1}k_{-2} + k_{-1}k_2 + k_{-1}k_3 + k_1k_2 + k_2k_{-3} + k_{-2}k_{-3} + k_1k_3 + k_1k_{-3} + k_{-2}k_3. \quad (13b)$$

In this system, ν_3 will still rise with the fast eigenrate m_5 and fall with the slow eigenrate m_4. Due to the fact that we have only two measurements directly relating to ν_3 and ν_6 and that this system contains three independent rate constants, it is an underdetermined system. However, an analysis based on this model provides some illuminating features relating to the CH_3Br system.

Acceptable values of k_1, k_2 and k_3 that will yield the observed m_4 and m_5 must now be expressed as a three-dimensional plot. Since the system is underdetermined by one observable, the acceptable solutions will fall on a curve. This curve is illustrated in fig. 6 for CH_3Br. Based on this model, it has been possible to find similar curves for all the rare gases so that the

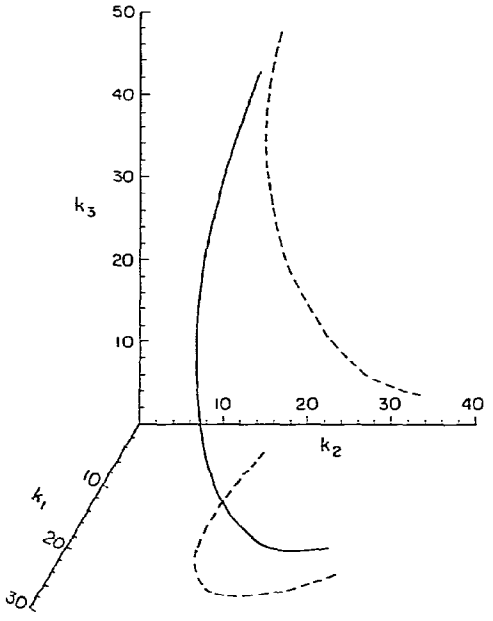

Fig. 6. Three dimensional plot of the solution of three-level model for methyl bromide including direct deactivation of ν_6. The solution has been obtained for pure methyl bromide where the observed rise rate (m_5) is 53.3 $ms^{-1}Torr^{-1}$ and the observed fall rate (m_4) is 19.5 $ms^{-1}Torr^{-1}$. The rate constants in the plot are also in units of $ms^{-1}Torr^{-1}$. The projections (dashed lines) of the solution (solid line) are also shown in order to aid interpretation. The rate constants refer to the processes indicated in fig. 7.

experimentally determined m_4 and m_5 are reproduced for each rare gas. However, as in the case of CH_3Br, if a unique set of rate constants is desired, an additional relationship must be established relating a pair of rate constants. It is interesting to note that solution sets exist for CH_3Br over a wide range of values of k_3, where k_3 can range from 3 to 47 $ms^{-1}Torr^{-1}$. At the upper limit k_3 is 8.6 times k_1, the value for direct deactivation of ν_3. Such large ratios of k_3/k_1 are probably unreasonable based on SSH and V→R theories. However, this qualification would only succeed in limiting us to the portion of the curve corresponding to smaller values of k_3/k_1.

Our extension of the system to include direct deactivation from ν_6 has now enabled us to determine a range of acceptable sets of rate constants which are consistent with the behavior of ν_3 for all the rare gases. However, other states exist in the CH_3Br system such as $2\nu_3$, which have populations that are comparable to ν_6 and additional information is available about the rise and fall of ν_2/ν_5. Thus it seems reasonable to extend the model to include these states, to determine their effect on the lower three states and to determine whether the available information dealing with ν_2/ν_5 will yield a unique set of rate constants. Where the selection of a unique set is not possible, the information regarding the behavior of ν_2/ν_5 may narrow the range of variation of one or more of the rate constants. The extension of the model to include ν_2/ν_5 and $2\nu_3$ will be attempted in steps.

4.2. *The four level system: $2\nu_3$, ν_6, ν_3 and ν_0*

The addition of $2\nu_3$ and the coupling of ν_3 to $2\nu_3$ via a non-linear step of the type

$$CH_3Br(\nu_3)+CH_3Br(\nu_3)\underset{k_{-4}}{\overset{k_4}{\rightleftharpoons}}CH_3Br(2\nu_3)+CH_3Br(0) \quad (14)$$

prevents a general analytic solution for the equilibration processes involving the lower four levels in fig. 7 [14]. Therefore the system must be solved numerically. The primary objective of the numerical treatment is to ascertain whether

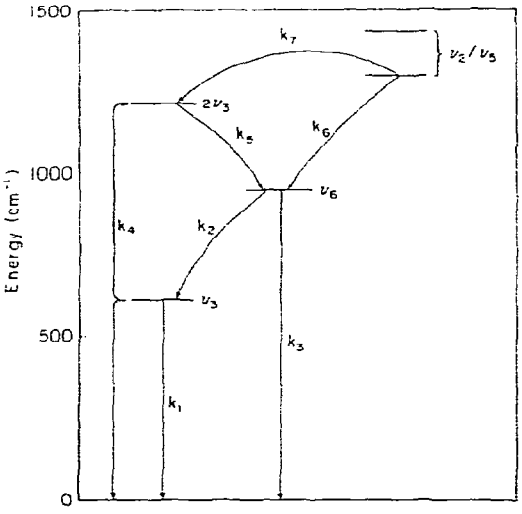

Fig. 7. Five-level model of methyl bromide. ν_2 and ν_5 have been combined and are considered to be a single state. The arrows indicate the forward direction of the rate equations in the text.

the addition of $2\nu_3$ to the system significantly affects the magnitude of the previously determined locus of rate constants for the three level system. In all of the treatments to follow we assume that k_4 is large, typically $1000\ \mathrm{ms^{-1}\ Torr^{-1}}$. This assumption is based on the large dipole moment derivative for the ν_3 mode which enters into a Sharma–Brau calculation of the magnitude of the near-resonant energy transfer cross section [16]. This type of calculation has been successful in reproducing the magnitude of the coupling between ν_3 and $2\nu_3$ in CH_3F where the corresponding rate constant has been measured experimentally [14, 17].

To treat the addition of $2\nu_3$, the numerical method described in appendix B was used. k_3 is fixed and the remaining rate constants in the system, k_1 and k_2 are then determined for different values of k_5 where k_5 is the rate constant coupling $2\nu_3$ and ν_6

$$\mathrm{CH_3Br}(2\nu_3)+\mathrm{CH_3Br} \underset{k_{-5}}{\overset{k_5}{\rightleftharpoons}} \mathrm{CH_3Br}(\nu_6)+\mathrm{CH_3Br}. \qquad (15)$$

In all cases treated for this system, an initial guess which resulted in a solution resulted in a unique solution.

Fig. 8 shows the solutions that are determined for an initial value of $k_3 = 16\ \mathrm{ms^{-1}\ Torr^{-1}}$. This value of k_3 is arbitrary but fig. 8 serves to illustrate the general effect of the addition of $2\nu_3$ on the previously determined set of rate constants. The first interesting observation is that there is a maximum allowable value for k_5. For the case of $k_3 = 16\ \mathrm{ms^{-1}\ Torr^{-1}}$, no solution sets for k_2 and k_3 can be found for $k_5 > 100\ \mathrm{ms^{-1}\ Torr^{-1}}$. The existence of an upper limit for k_5 is not too surprising since there appears to be a tradeoff in magnitude between k_2 and k_5. This tradeoff is present for all allowed values of k_3. The tradeoff appears to occur because processes 2 and 15 both represent ways to deplete ν_6 in population and to populate ν_3. The parallelism of the two processes is further inferred by the observation that the magnitude of k_1, the rate constant for V→T/R deactivation of ν_3, varies little as a function of k_5. Similar behavior is observed for all allowed values of k_3 that were tested. Thus for CH_3Br, though the inclusion of $2\nu_3$ and its coupling to ν_6 affects the possible values of k_2 for a given k_3, the values of k_1 for each k_3 remain essentially unchanged. However, as before, there are still families of acceptable

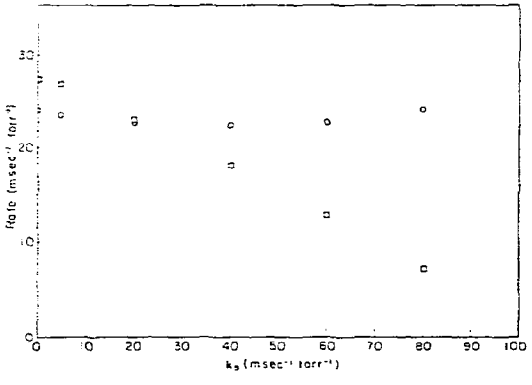

Fig. 8. Rate constants k_1 (circles) and k_2 (squares) are plotted versus k_5. k_3 has been fixed at 16 and k_4 fixed at $1000\ \mathrm{ms^{-1}\ Torr^{-1}}$. The rates shown in the plot are for 1 Torr of methyl bromide.

values for k_1 and k_3; and the addition of $2\nu_3$ does not help us determine which sets of rate constants actually occur.

From the results of the numerical study of the four level system presented above, it can be concluded that the kinetic processes involving $2\nu_3$, ν_6, ν_3 and ground state of CH_3Br can be adequately treated by three independent rate constants, k_1, k_2 and k_3. This is accomplished by setting $k_4 = 1000\ \mathrm{ms^{-1}\,Torr^{-1}}$, and by taking advantage of the complementary relation between k_2 and k_5 which allows us to choose a value for k_2 which represents the combination of the two kinetic processes. Doing this allows us to effectively set $k_5 = 0$ in our model. This model will be assumed in the following development.

4.3. *The five level system: ν_3, ν_6, $2\nu_3$, ν_2/ν_5, ν_0*

The population of ν_2/ν_5 is small compared to that of ν_3 and ν_6. Thus the rate processes involving ν_2/ν_5 represent a small perturbation on the lower manifold and would not be expected to significantly alter the values of rate constants determined in the four level model. For the same reason, the behavior of ν_2/ν_5 reflects the rate processes involving ν_3 and ν_6 very closely, through the rate constants tying ν_2/ν_5 to the lower manifold. The addition of ν_2/ν_5 to the four level model described in the previous section introduces two additional observables, namely the rise and fall of ν_2/ν_5. However, two new rate constants, k_6 and k_7, are also added to the model as independent variables. Therefore, as in the four level model, this five level model is also underdetermined by one observable. While the model cannot be expected to uniquely define any of the rate constants involved in the system, it will be shown that the introduction of ν_2/ν_5 limits the acceptable range of values of rate constants, in particular those of k_1 and k_3.

Fig. 9 is a plot of the various rate constants obtained from the different models. The abscissa of the plot is the value of the $\nu_6 \rightarrow 0$ rate constant, k_3, which is taken as the independent variable. For a given value of k_3, the four

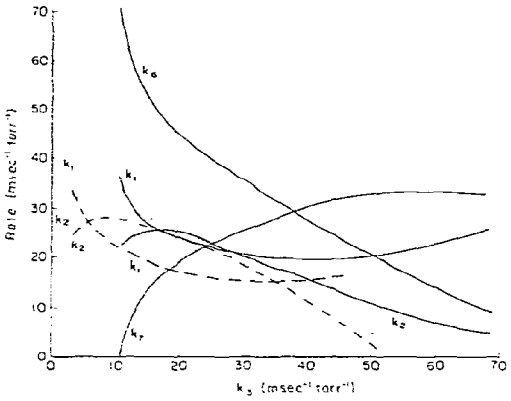

Fig. 9. The development of the methyl bromide kinetic model is depicted where k_1 and k_2 are plotted versus k_3. The rate constants have been obtained from the three level model (–·–) without direct deactivation of ν_6, the four-level model (···) and the five-level model (——). k_6 and k_7 are included for the five-level model.

rate constants, k_1, k_2, k_6 and k_7, that generate the observed rates are obtained by the method described in appendix B.

An interesting observation is the similar shape of the curves in fig. 9 for k_1 and k_2 for all models. Though there is certainly some translation of the curves in both the x and y direction it is clear that similar values of k_2 and k_1 are expected for each value of k_3 for all models used. This is a demonstration of the fact that inclusion of upper levels will not, in general, dramatically alter the behavior of lower states due to the small population of these upper states.

Another prediction of the five-level model is the finite magnitude of the relaxation step involving direct deactivation of ν_6. It can be seen in fig. 9 that for $k_3 < 10.6\ \mathrm{ms^{-1}\,Torr^{-1}}$; $k_7 < 0$. It can therefore be concluded that the mean minimum allowed value for k_3 is $10.6\ \mathrm{ms^{-1}\,Torr^{-1}}$. The statistically acceptable minimum value of k_3 can be calculated by first setting $k_7 = 0$ which, as seen in fig. 9 defines the minimum of k_3 and then calculating the error bars and the mean of k_3 via the method of appendix A. k_3 is then calculated as $11.6 \pm 5.2\ \mathrm{ms^{-1}\,Torr^{-1}}$ where the indicated error is the

95% confidence limit. Thus from this error limit calculation 6.4 $ms^{-1} Torr^{-1}$ is the statistically acceptable minimum value for the deactivation of ν_6. The difference that occurs in the calculation of the mean of k_3 via the method of appendix A and the mean of k_3 as shown in fig. 9 is due to the statistical weighting that is incorporated in the former calculation which does not exist in the latter calculation. By either method it can be asserted that in pure CH_3Br there is a significant direct deactivation step for the ν_6 mode.

Considerations that can be used to establish an upper limit for this rate constant and allow for the selection of a reasonable range of variation of the other rate constants will be discussed next. To do this, more information is necessary to make a judgment about the allowable relative or absolute magnitudes of rate constants.

One method of doing this is to resort to theoretical calculations of the relative rates of k_1 and k_2. Whereas the absolute magnitude of theoretically calculated rate constants may be significantly in error, relative magnitudes of theoretically calculated rate constants often agree with experimental data [11, 12, 18]. An SSH calculation of rates of deactivation of ν_3 and ν_6 in CH_3Br–CH_3Br and CH_3Br–rare gas collisions is given in table 2. From these calculations it is clear that though significant direct deactivation of ν_6 in CH_3Br would be expected to occur for light collision partners, direct deactivation of ν_6 is minimal for the heavy collision partners. SSH theory considers a perturbation involving relative translational motion [18]. In systems in which the relative rotational velocity is greater than the relative translational velocity, V→R energy transfer calculations may be more relevant in a calculation of relative relaxation rates. A measure of the relative magnitude of the rotational versus translational velocity for a specific system is given by $(\mu d^2/I)^{1/2}$ which, if greater than 1, has been shown to indicate a significant role for V→R processes in the relaxation of a molecule [11]. As seen in table 3, this quantity is greater than or equal to 1 (0.98 for ^3He) for all collision partners studied and increases as the mass of the collision partner increases. Thus, V→R calculations of the relative rates of k_1 and k_3 via the model of ref. [11] seem warranted. Using eq. (9) of ref. [11] and assuming α (the repulsive exponential range parameter) is constant for all collision partners, the ratio Z_1/Z_3 was calculated to be 2.5, where Z_k is the collision number associated with the process k.

It is important to note that existing theoretical models predict k_3 to be less than k_1. Thus it seems reasonable to accept $k_3/k_1 = 1$ as an upper limit. For $k_3/k_1 = 1$, the upper limit of k_3 can be obtained from fig. 9 as ≈ 24 $ms^{-1} Torr^{-1}$. This limits the acceptable region of the solutions of the five-level model presented in fig. 9 to k_3 values of 10.6–24 $ms^{-1} Torr^{-1}$ with error limits on the lower bound of this range as discussed above.

Table 2
Theoretical energy transfer probabilities calculated via the SSH method [18] for the V→V and V→T processes in CH_3Br

Collision partner	Process					
	$\nu_3 \rightarrow 0$	$\nu_6 \rightarrow 0$	$\nu_6 \rightarrow \nu_3$	$\nu_6 \rightarrow 2\nu_3$	$\nu_{2,5} \rightarrow \nu_6$	$\nu_{2,5} \rightarrow 2\nu_3$
CH_3Br	2.36×10^{-5}	1.91×10^{-7}	8.03×10^{-4}	2.38×10^{-5}	2.25×10^{-3}	1.41×10^{-3}
^3He	2.35×10^{-2}	4.05×10^{-2}	1.02×10^{-2}	6.64×10^{-5}	3.37×10^{-2}	2.05×10^{-4}
^4He	1.93×10^{-2}	2.55×10^{-2}	1.05×10^{-2}	7.28×10^{-5}	3.44×10^{-2}	2.52×10^{-4}
Ne	1.77×10^{-3}	2.88×10^{-4}	5.62×10^{-3}	7.37×10^{-5}	1.73×10^{-4}	7.63×10^{-4}
Ar	3.8×10^{-4}	1.56×10^{-5}	3.49×10^{-3}	4.28×10^{-5}	6.85×10^{-3}	9.94×10^{-4}
Kr	2.8×10^{-5}	3.08×10^{-7}	7.71×10^{-4}	2.15×10^{-3}	2.2×10^{-3}	1.09×10^{-3}
Xe	4.18×10^{-6}	1.62×10^{-8}	2.44×10^{-4}	3.66×10^{-4}	6.69×10^{-4}	3.22×10^{-2}

Table 3
The reduced mass and ratio of translational to rotational velocities $(\mu d^2/I)^{1/2}$ for CH_3Br–rare gas pairs [a]

Collision partner	Reduced mass (amu)	$(\mu d^2/I)^{1/2}$
^3He	2.91	0.98
^4He	3.84	1.12
Ne	16.64	2.34
Ar	28.12	3.05
Kr	44.5	3.83
Xe	55.1	4.27

[a] $d = 1.048$ Å, $I = 3.386$ amu Å^2.

In order to study the rare gas dependent rate constants, a choice has to be made for k_3, or equivalently for k_3/k_1, in neat CH_3Br. Based on the above calculations, a k_3/k_1 value of 0.4 is chosen for this purpose. The five-level model rate constants corresponding to this choice, in neat CH_3Br are: $k_1 = 29.9$, $k_2 = 26.8$, $k_3 = 12.0$, $k_4 = 1000$, $k_5 = 0.0$, $k_6 = 55.1$ and $k_7 = 21.0$, all reported in units of ms^{-1} (Torr $CH_3Br)^{-1}$.

It should be pointed out that future experimental studies could, in all likelihood, be performed which would obviate the need for the above assumptions which are now based on theoretical calculations. Additional information could be obtained by measuring the rise and fall of the ν_6 state or by looking at the relative amplitude of the ν_3 and ν_2/ν_5 states and how these amplitudes change as a function of pressure. Numerical models of the system have confirmed that either of these measurements could, in principle, greatly limit the acceptable range of solution sets. However, both of these possibilities have experimental difficulties associated with them. In the case of ν_6, the presence of laser scatter will make observation of this relatively weakly emitting state quite difficult. Measurement of intensities is always a difficult experimental problem due to changes in self-trapping and absorption coefficients with pressure. However, photoacoustic detection could be used to normalize for absorption coefficient changes and it seems likely that with sufficient effort either study could be performed. The results of either of these studies would then experimentally limit possible solution sets for methyl bromide and methyl bromide–rare gas systems to a narrow range.

4.4. CH_3Br rare gas processes

Once a set of parameters is established for use as CH_3Br–CH_3Br rate constants, the same five-level kinetic scheme can be used in an effort to determine rare gas–CH_3Br kinetic rate constants. Rare gas rate constants will be designated by k^* with a subscript referring to the same process as it refers to in fig. 7 for pure CH_3Br. Of course, for the rare gases, $k_4^* = 0$, since a resonant process does not exist for the population of $2\nu_3$. The kinetic rate equations for the rare gases are still underdetermined, since, as in the case of pure CH_3Br, there are four kinetic rate measurements and five unknowns. Again, a convenient approach is to choose a value for k_3^* and solve the kinetic equations for the remaining four rate constants. This has been done for different values of k_3^*. The corresponding k_1^* for each rare gas collision partner is displayed in fig. 10.

Though varying the value of k_3^* does affect the value of k_1^*, it is clear that the shape of the plot of k_1^* versus $\mu^{1/2}$ will be essentially the same virtually independent of the magnitude of k_3^* over the ranges treated in fig. 10. The only significant change in the shape of the plot would result if k_3^*/k_1^* for ^3He and ^4He were substantially greater than 1.

It is now possible to ask how a change in the assumed magnitude of the CH_3Br k_3 rate constant would effect k_1^*. This was investigated by setting $k_3^* = 0$, varying k_3, and solving the rate equations for the different rare gas rate constants. For argon for $k_3 = 20$, 30, 40; $k_1^* = 3.76$, 3.25, 2.80 ms^{-1}, respectively. These results were typical of the other rare gases. From this, it is clear that even a factor of two variation in the magnitude of k_3 will result in only a $\approx$30% change in k_1^*. In these calculations, $k_3^* = 0$ was chosen for convenience.

In formulating fig. 9 it was found that while a direct deactivation of ν_6 is mandated from the data for CH_3Br–CH_3Br collisions, a direct

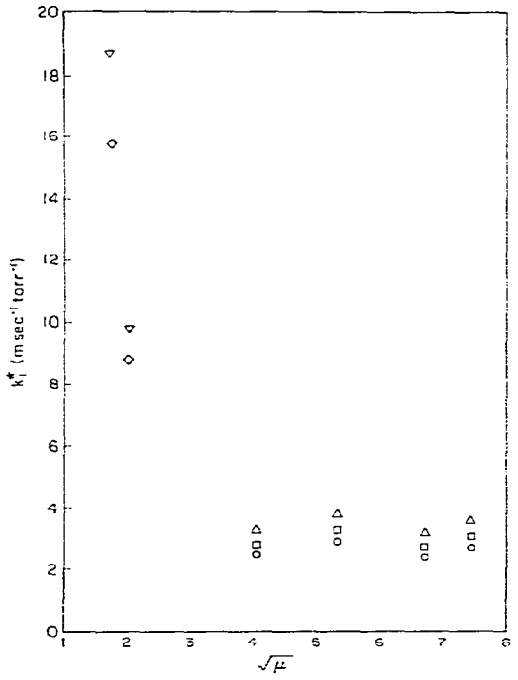

Fig. 10. The dependence of the rate constant k_3^* on k_1^* for the rare gas collision partners. The numbers were generated from a five-level model for methyl bromide. The symbols represent different values of k_5^* (where $\nabla = 4$, $\diamond = 8$, $\triangle = 0$, $\square = 0.5$ and $\bigcirc = 1.0$).

deactivation of ν_6 does not appear to be necessary for all the rare gases to obtain a solution to the rate equations. For ^{3}He a direct deactivation of ν_6 is necessary while for ^{4}He the situation is marginal with respect to the necessity of a direct deactivation of ν_6. This does not necessarily imply that a direct deactivation of ν_6 by the heavy rare gases does not occur, but rather it may be that the solution to the rate equations for the heavy rare gases have a wider range of possible solution sets for the light rare gases. Indeed, the fact that $(\mu d^2/I)^{1/2}$ increases with the mass of the rare gas implies that rotations are more important for the heavier rare gases. If simple V→R theory is then applied to these gases, a significant direct ν_6 deactivation rate relative to the ν_3 rate would be predicted.

As previously stated, data on the experimentally observed rates of deactivation of CH_3Br were reported in ref. [7]. Theoretically calculated rate constants were compared to these rates in ref. [12] by making the following calculation

$$R_{\text{obs}} = \frac{N_{\nu_3}}{N_{\nu_3} + N_{\nu_6}} k_{\nu_3} + \frac{N_{\nu_6}}{N_{\nu_3} + N_{\nu_6}} k_{\nu_6}, \tag{16}$$

where N_{ν_6} is the population of state ν_i and k_{ν_i} is the calculated deactivation rate from state ν_i. R_{obs} is the calculated observed deactivation rate. Applying eq. (16) to calculated rate constants in an effort to reproduce experimental data relies on the assumption that ν_3 and ν_6 are equilibrated on a timescale much shorter than the deactivation timescale. This was a reasonable assumption lacking further information (though reverse rate constants should also be included), but as we have shown above, is not what occurs in the CH_3Br system. Thus a meaningful comparison of theory and experiment in this system can only be done by comparing individual rate constants. Fig. 9 presents our best estimate of the ν_3 and ν_6 deactivation rate constants for CH_3Br–X collisions and this figure and the accompanying text discuss possible ranges for these rate constants. Similar data are presented for CH_3Br–CH_3Br collisions. The corresponding theoretically calculated individual rate constants for deactivation of ν_3 and ν_6 have not been published. Thus, a direct comparison is not possible at this time. It is possible to compare the quantity calculated by using eq. (16) with our rate constants as inputs with published theoretical values of the same quantity. However, since ν_3 and ν_6 do not rapidly equilibrate the quantity calculated via eq. (16) is not physically meaningful and thus this comparison was not attempted.

It is appropriate, at this point, to scrutinize the vibrational energy transfer studies on the methyl halide series. In the case of CH_3F, the timescale of vibration–vibration energy transfer processes are well separated from the timescale of vibrational relaxation processes. In this case, the actual rate of vibrational relaxation will be related to the sum of the forward and backward

rate constants for relaxation if relaxation occurs from a single state. In CH_3F there is evidence that relaxation occurs from both the ν_3 and ν_6 states. Under these circumstances, the measured rate will be a weighted sum of the forward and backward rate constants of both states. This case has been treated in ref. [15] and no re-evaluation is necessary for CH_3F.

CH_3Cl is an intermediate case in that the timescale for V–V processes is an order of magnitude greater than for V→T/R processes [19]. This will mean that, assuming the system involves basically the same kind of transfer processes as in CH_3Br, the measured rates will not be merely the sum of the forward and backward V→T/R rate constants. Thus some correction will be necessary for the effects of V–V rates. However, in this system these corrections are likely to be small.

CH_3I represents a potentially complex system in which, as in CH_3Br, V–V rates are quite close to V→T/R rates [20] and thus this system will have to be subjected to an analysis as done herein for CH_3Br in order to determine actual kinetic rate constants.

Despite the above comments we feel that the general picture of relaxation in which for light rare gases V→T and V–R processes are important and V–R processes become dominant for heavy rare gases with V→R relatively more important for the heavier CH_3X's will persist [7]. This conclusion is based on the results of the reanalysis of CH_3Br and calculations of relative translational versus rotational velocities for the CH_3X's undergoing rare gas collisions.

5. Conclusions

We have outlined a method and a procedure which allows for the extraction of kinetic rate constants from measured rates in a complex polyatomic system. In the course of this procedure, we have developed a numerical method which can determine kinetic rate constants from measured rates by the iterative solution of a set of coupled rate equations. As a result of this study, we have determined that there is a significant rate for direct deactivation of ν_6 to the ground state of CH_3Br in CH_3Br–CH_3Br collisions in addition to the "normal" deactivation of ν_3. We have determined acceptable solution sets for the kinetic rate equations for CH_3Br. When the ratio of k_1/k_3 calculated from theory is included as an input to the kinetic model, the range of solution sets for the CH_3Br rate constants is narrowed. With this solution set as a starting point, sets of rate constants can be obtained for CH_3Br–rare gas interactions. The effect of variation in the initial set of CH_3Br–CH_3Br rate constants on the set of CH_3Br–rare gas rate constants was considered.

We have also explicitly considered the propagation of errors from experimental rates to kinetic rate constants in the three level system. We have shown that use of the normal approximate analytic expression for propagation of errors in a complex system can result in significant errors in the calculations of error limits on rate constants. We present an exact numerical method for calculation of error limits on rate constants.

The necessity for a kinetic reanalysis of the other methyl halides has been considered. It is likely that the previous conclusions drawn regarding the mechanism of deactivation of the methyl halides will not change. However, while the existing interpretation of the data on CH_3F deactivation rate constants is valid, on reanalysis the interpretation of the data on CH_3Cl would change, though only by a small amount and CH_3I should be subjected to a full reanalysis.

Appendix A

It is common practice to report the experimental error on measured rates. Though the situation is changing [22–24], historically little attention has been paid to the propagation of these errors to produce appropriate error limits on the derived kinetic rate constants. Since, as shown in eq. (5), the observed rate is a complex function of rate constants, the error on the rate constants would also be expected to be a com-

plex function of both the error limits on the observed rates as well as the actual magnitude of the observed rates. A treatment involving propagation of experimental errors on observed rates to actual errors on rate constants has been previously presented for a specific type of four level system [21]. Since a three level system is very frequently used as a kinetic model, a discussion of error limits on rate constants for this system would be appropriate. Additionally we will comment on the validity of the commonly used technique for a propagation of error analysis and present a technique which can be applied to virtually any system.

A standard error treatment involves expressing the variance of a rate constant in the three level system described by eq. (1) as

$$V_{k_2}=(\partial k_2/\partial m_1)^2 V_{m_1}+(\partial k_2/\partial m_2)^2 V_{m_2}, \qquad (A.1)$$

where

$$\frac{\partial k_2}{\partial m_1}=\frac{1}{2y}\pm\left(\frac{m_1+m_2}{2y^2}-\frac{zm_2}{yx}\right)\times\left[\left(\frac{m_1+m_2}{y}\right)^2-\frac{4zm_1m_2}{xy}\right]^{-1/2} \qquad (A.2)$$

and

$$\frac{\partial k_2}{\partial m_2}=\frac{1}{2y}\pm\left(\frac{m_1+m_2}{2y^2}-\frac{zm_1}{yx}\right)\times\left[\left(\frac{m_1+m_2}{y}\right)^2-\frac{4zm_1m_2}{xy}\right]^{-1/2}. \qquad (A.3)$$

A similar expression can be derived for V_{k_1} where

$$\frac{\partial k_1}{\partial m_1}=\frac{1}{2z}\pm\left(\frac{m_1+m_2}{2z^2}-\frac{ym_2}{xz}\right)\times\left[\left(\frac{m_1+m_2}{z}\right)^2-\frac{4ym_1m_2}{xz}\right]^{-1/2} \qquad (A.4)$$

and

$$\frac{\partial k_1}{\partial m_2}=\frac{1}{2z}\pm\left(\frac{m_1+m_2}{2z^2}-\frac{ym_1}{xz}\right)\times\left[\left(\frac{m_1+m_2}{z}\right)^2-\frac{4ym_1m_2}{xz}\right]^{-1/2}, \qquad (A.5)$$

where x, y and z are defined as

$$x=k_{-1}k_{-2}+k_{-1}k_2+k_1k_2,$$

$$y=k_1+k_{-1},$$

$$z=k_2+k_{-2}.$$

Fig. 11 shows the percent error in the rate constants k_1 and k_2, calculated via eqs. (A.1)–(A.5), that result from a 1% error in m_1 and m_2. The abscissa is a plot of m_1 for a fixed value of m_2 ($m_2=1$) for the CH_3Br system. It is interesting to note that as m_1/m_2 approaches its minimum value for this system, the errors on the rate constants become relatively large for a given error on the rates.

As pointed out in ref. [22], the application of eq. (A.1) assumes that the values of the partial derivative in eq. (A.1) are constant with respect to changes in the observed rates over their range of errors. In fact, the value of the partial derivatives are not necessarily constant over the limits of error, nor do they vary linearly over this range. Therefore eq. (A.1) can only give an approximate error on the rate constants. Ref. [22] presents a more accurate method for estimation of the errors that are suitable for application to kinetic modeling. The procedure was adopted for use in the present CH_3Br study by incorporating the techniques developed in appendix B. The procedure of obtaining the errors of the rate constants is to add to each observed rate the product of the error of that rate, σ, and a random number of gaussian distribution with unity standard deviation, R.

$$B_j^*=B_j+\sigma_jR, \qquad (A.6)$$

where a new random number is produced for each observed rate. The set of modified observed rates B^* is then used in the solution of the rate constants as described in appendix B. The rate constants resulting from this solution are saved and eq. (A.6) is again used to alter the observed rates and a new set of rate constants are produced. This procedure is repeated until a large sampling of rate constants have been generated. The errors of each of the rate constants being solved for can then be determined by standard error analysis of the sampling of these

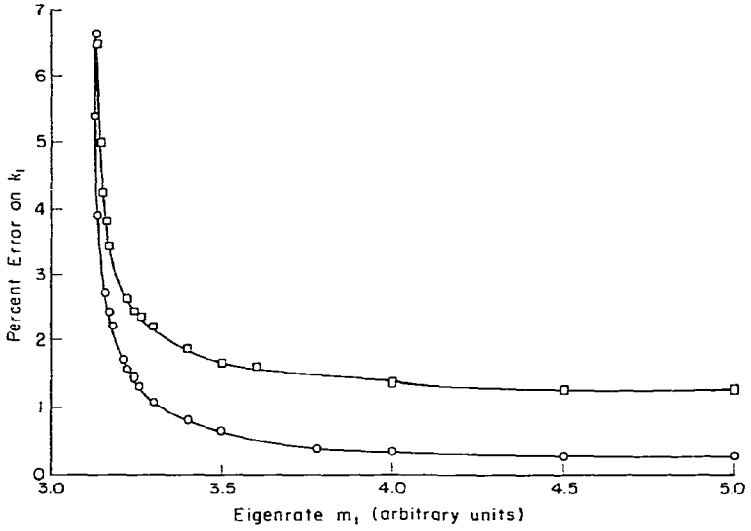

Fig. 11. Error propagation in a three-level kinetic model. The percent error in k_1 is plotted versus the value of the eigenrate m_1. m_2 is taken as equal to 1. The two lines represent the two possible solutions for k_1 in eq. (A.2). The □ represents the + solution and the ○ the − solution. In both cases a 1% experimental error is assumed on m_1 and m_2.

rate constants. This numerical procedure was tested by comparison to the results of eqs. (A.1)–(A.5). The agreement was very good when the errors on the observed rates were small. It was also confirmed that good agreement between the numerical and analytical results was only obtained for relatively small (<10%) errors on the observed rates.

Though the numerical approach can involve significant additional computation, it has the advantage that errors on the rate constants can be obtained from any numerically soluble kinetic model. Thus it is not limited to systems for which there are analytical expressions existing which relate the observed rates to the rate constants.

The length of the computation can be significant. For example using a NOVA/4 computer, the estimation of the error for four rate constants for the five level system described in the text took anywhere from 10 min to a more typical 12 h. The variance in these execution times is primarily related to the amount of experimental error on the observed rates. The correlation of long execution times and larger error on the observed rates is a direct result of the need to re-evaluate the partial derivatives as discussed in appendix B. Therefore it is somewhat consiliatory that the longer the execution time, the less reasonable the analytical solution for the errors.

Appendix B

One goal of energy transfer studies is to determine if a proposed model can be used to reproduce an observed set of rates. The model can be represented as a set of coupled rate equations,

$$dN_j/dt = \sum k_i N_i, \tag{B.1}$$

which can be made to simulate the experiment by initially perturbing the appropriate populations and then solving eq. (B.1) for a given set of rate constants. The solution can be obtained by either analytical or numerical techniques.

The following discussion will pertain to the results from a numerical solution since it is more easily applied to a variety of problems. The result of a numerical solution is a time dependent variation of population which can be directly compared to an experimental signal. In order to facilitate this comparison, it is useful to extract the eigenrates from both the model generated and experimentally obtained signals. The relationship between the observed signal and the eigenrates R_n is described by:

$$N_i(t) = \sum_n P_n \exp(-R_n t), \tag{B.2}$$

where P_n is the eigenvector or the preexponential. R_n will be represented for the model and for the experimental results as A_n and B_n, respectively. The eigenrates can be obtained by either the NLSQ or the Guggenheim techniques that have been discussed in the text.

The objective of modelling is to obtain sets of rate constants for eq. (B.1) such that all eigenrates A_n are equal to the corresponding B_n, i.e., there is agreement between the model and the experiment. Though some progress has been made in this area, traditionally the desired rate constants have been obtained by a trial and error process where (B.1) is solved using an initial guess for the rate constants. The resulting signal is compared to the experimental results and if there is any significant discrepancy the rate constants are changed and (B.1) is solved again. This process is repeated until it is felt that there is either sufficient equivalence between A_n and B_n or that no reasonable solution is possible.

An algorithm that will directly produce the desired set of rate constants has been used in our studies. Its principle advantage is the reduction of both the tedium and the subjectivity imposed by the above procedure. Additionally, it makes the numerical error analysis discussed in appendix A feasible.

The procedure is to solve (B.1) by using an initial guess for the rate constants. The difference between the corresponding rates A_n and B_n can be attributed to a sum of error terms.

$$B_n - A_n = \sum_{j=1}^{m} (\partial A_n/\partial k_j)\Delta k_j, \tag{B.3}$$

where Δk_j is the difference between the desired jth rate constant and its current estimate. Eq. (B.3) is a result of the Newton–Raphson scheme for solving nonlinear equations [24].

The partial derivatives in eq. (B.3) are elements of a jacobian matrix. The jacobian can be generated by either analytical or numerical techniques. Since numerical techniques are of most general application, we will consider how to generate the elements of the jacobian matrices by a numerical method. The partial derivatives can be approximated by:

$$\partial A_n/\partial k_j = \delta^{-1}[A_n(\ldots k_{j-1}, k_j+\delta, k_{j+1}\ldots) - A_n(\ldots k_{j-1}, k_j, k_{j+1}\ldots)],$$

where n and j are respectively the row and column indices of the jacobian matrix. The magnitude of δ is chosen to be a small fraction of the magnitude of the rate constants to be varied. Its actual value depends on the accuracy of the evaluation of A_n. In our calculations δ was 2–5% of the median of the rate constants being varied and was not changed during the execution of the program. A_n was obtained by the iterative Guggenheim technique that has been presented in the text.

Δk can be obtained by simultaneous solution of the following m linear equations:

$$\begin{aligned} B_1 - A_1 &= \sum_{j=1}^{m} (\partial A_1/\partial k_j)\,\Delta k_j, \\ &\vdots \\ B_m - A_m &= \sum_{j=1}^{m} (\partial A_m/\partial k_j)\,\Delta k_j, \end{aligned} \tag{B.4}$$

where m is the total number of observed eigenrates.

The desired rate constants, k^+, are obtained by

$$k_j^+ = k_j + \Delta k_j S. \tag{B.5}$$

Since the partial derivatives in eq. (B.4) are generally not constant with respect to changes in the rate constants, k_j^+ is only an estimate of the desired rate constants. For this reason, eq. (B.1) must be repeatedly reevaluated, each time using a jacobian matrix that has been generated

for the most recent estimates of the rate constants. This iterative solution is repeated until divergence is detected or there is satisfactory agreement between eigenrates A and B. Satisfactory agreement in the methyl bromide study was taken as all of the modelled eigenrates being within 1% of the corresponding experimental eigenrates. Another consequence of the partial derivatives not being constant is the Δk may grossly overcorrect the rate constants. Therefore a damping factor, S, was included to stabilize the convergence of the solution. The value of S used in our calculations was ≈ 0.5.

Acknowledgement

We gratefully acknowledge support of this work by the National Science Foundation under grant CHE 79-08501.

References

[1] T.L. Cottrell and J.C. McCoubrey, Molecular energy transfer in gases (Butterworths, London, 1961).
[2] J.D. Lambert, Vibrational and rotational relaxation in gases (Clarendon Press, Oxford, 1977).
[3] J.L. Stretton, Transfer and storage of energy by molecules, Vol. 2. Vibrational energy, eds. G.M. Burnett and A.M. North (Wiley–Interscience, New York, 1969).
[4] J.T. Yardley, Introduction to molecular energy transfer (Academic Press, New York, 1980).
[5] (a) C.B. Moore, Advan. Chem. Phys. 23 (1973) 41; (b) C.B. Moore, Ann. Rev. Phys. Chem. 22 (1971) 387.
[6] (a) E. Weitz and G.W. Flynn, Ann. Rev. Phys. Chem. 25 (1974) 275; (b) G.W. Flynn, in: Chemical and biochemical applications of lasers, Vol. 1, ed. C.B. Moore (Academic Press, New York, 1977); (c) E. Weitz and G.W. Flynn, Photoselective Chemistry Part II, Adv. Chem. Phys. Ser. 185 (1981).
[7] B.L. Earl, L.A. Gamss and A.M. Ronn, Acc. Chem. Res. 11 (1978) 183.
[8] B.L. Earl and A.M. Ronn, Chem. Phys. 12 (1976) 113.
[9] G.T. Fujimoto and E. Weitz, Chem. Phys. 27 (1978) 65.
[10] E.A. Guggenheim, Phil. Mag. 2 (1926) 538.
[11] C.B. Moore, J. Chem. Phys. 43 (1965) 2979.
[12] (a) R. Zygan-Maus and S.F. Fischer, Chem. Phys. 41 (1979) 319; (b) A. Miklavc and S.F. Fischer, J. Chem. Phys. 69 (1978) 281; (c) A. Miklavc, J. Chem. Phys. 72 (1980) 3805.
[13] T.M. Lowry and W.T. John, J. Chem. Soc. (London) 97 (1910) 2634.
[14] V.A. Apkarian and E. Weitz, J. Chem. Phys. 71 (1979) 4349.
[15] E. Weitz and G.W. Flynn, J. Chem. Phys. 58 (1973) 2781.
[16] R.D. Sharma and C.A. Brau, J. Chem. Phys. 50 (1969) 924.
[17] R.S. Sheorey and G.W. Flynn, J. Chem. Phys. 72 (1980) 1175.
[18] R.N. Schwartz, Z.I. Slawsky and K.F. Herzfeld, J. Chem. Phys. 20 (1952) 1951.
[19] J.T. Knudtson and G.W. Flynn, J. Chem. Phys. 58 (1973) 2684.
[20] Y. Langsam, S.M. Lee and A.M. Ronn, Chem. Phys. 14 (1976) 375.
[21] M.I. Lester and G.W. Flynn, J. Chem. Phys. 72 (1980) 6424.
[22] C.G. Swain, M.S. Swain and P.F. Strong, J. Chem. Inf. Comput. Sci. 20 (1980) 51.
[23] M. Demiralp and H. Rabitz, J. Chem. Phys. 74 (1981) 3362.
[24] C.F. Gerald, Applied numerical analysis (Addison-Wesley, Reading, 1978).